Understanding patterns of distribution shifts and range expansion/contraction for the small yellow croaker (*Larimichthys polyactis*) population of the Yellow Sea

Qingpeng Han[1, 2, a], Arnaud Grüss[3, b], Xiujuan Shan[1, 4, c*], Xianshi Jin[1, 4, d], James T. Thorson[5, e]

[1]Key Laboratory of Sustainable Development of Marine Fisheries, Ministry of Agriculture, Shandong Provincial Key Laboratory of Fishery Resources and Ecological Environment, Yellow Sea Fisheries Research Institute, Chinese Academy of Fishery Sciences, Qingdao 266071, China

[2]College of Fisheries, Ocean University of China, Qingdao 266003, China

[3]School of Aquatic and Fishery Sciences, University of Washington, Box 355020, Seattle, WA, 98105-5020, USA

[4]Function Laboratory for Marine Fisheries Science and Food Production Processes, Qingdao National Laboratory for Marine Science and Technology, Qingdao 266237, China

[5]Habitat and Ecological Processes Research program, Alaska Fisheries Science Center, National Marine Fisheries Service, NOAA, 7600 Sand Point Way N.E., Seattle, WA 98115, USA

Author email addresses
[a]qhan@foxmail.com
[b]gruss.arnaud@gmail.com
[c]shanxj@ysfri.ac.cn
[d]jin@ysfri.ac.cn
[e]james.thorson@noaa.gov

Keywords: Distribution shifts; effective area occupied; Yellow Sea; small yellow croaker.

Funding: This work was supported in part by the National Research Program of China [2017YFE0104400]; the National Natural Science Foundation of China [31872692]; the National Basic Research Program of China [2015CB453303]; the Taishan Scholar Project; and the "Aoshan Talent" Project Financially Supported by the Qingdao National Laboratory for Marine Science and Technology [2017ASTCP-ES07]. The funders had no role in study design, data collection and analysis, decision to publish, or preparation of the manuscript.

Corresponding author
Dr. Xiujuan Shan
Yellow Sea Fisheries Research Institute
Chinese Academy of Fishery Sciences
Qingdao 266071, China
Telephone: 0532-85812159
Email: shanxj@ysfri.ac.cn

ABSTRACT

Detecting and understanding patterns of distribution shifts and range expansion/contraction for fish populations is important to explore potential mechanisms for population dynamics and communicate changes in stock status. In this study, we developed a spatio-temporal model for the small yellow croaker ("yellow croaker"; *Larimichthys polyactis*) population of the Yellow Sea for the period 2001-2017. This model was fitted to biomass catch rate data collected by the fixed-station bottom trawl surveys conducted in the Yellow Sea in the winter (January) of 2001–2011 and 2015–2017. The spatio-temporal model accounts for both spatial and spatio-temporal structure at a fine scale, and can potentially include the effects of sea surface temperature and of an annual index, the Pacific Decadal Oscillation, which is represented using a recently-developed spatially-varying coefficient model. We employed the spatio-temporal model to estimate changes in the northward and eastward centers of gravity (COGs) and effective area occupied of yellow croaker over the period 2001-2017, to reveal patterns of distribution shifts and range expansion/contraction for the species. We selected a spatio-temporal with no covariates based on Akaike's Information Criterion. This model estimated that the COG of yellow croaker moved north and west between 2001 and 2010, and then south and west over the period 2010-2017. Only the westward shifts of yellow croaker COG were found to be statistically significant. These results reflected the progressive disappearance of yellow croaker density hotspots (i.e., highest density areas) in the north and southeast areas of the Yellow Sea that was predicted by the spatio-temporal model, which resulted in the central area of the Yellow Sea becoming the only yellow croaker density hotspot in 2017. This finding has important implications for fisheries management in the context of the China-South Korea fisheries agreement, as it indicates a measurable displacement of yellow croaker biomass towards China. The spatio-temporal model developed in this study is one of the first for the Yellow Sea, and it is the first

72 spatio-temporal model for the Yellow Sea that implements a spatially-varying coefficient
73 model to represent the effects of an annual index, namely the PDO. Our spatio-temporal
74 modeling framework will allow for investigations for other species that inhabit the Yellow
75 Sea and will contribute valuable information about essential fish habitats (e.g., spawning and
76 nursery grounds) and their spatial evolution, thereby supporting the development of spatial
77 protection plans and other resource management measures for the Yellow Sea.

1. Introduction

Detecting and understanding patterns of distribution shifts and range expansion/contraction for fish populations is important for effective resource management. This understanding can facilitate the development of adaptative and flexible monitoring programs that appropriately sample fish populations and, thereby, provide reliable data to stock and habitat assessments (Karp et al., 2019). It can also help scientists and resource managers anticipate potential changes in the productivity of fish stocks and marine ecosystems and in fisheries catches, and foresee management measures accordingly (Cheung et al., 2009, 2012).

Evidence is accumulating that anthropogenic (e.g., fishing) and/or environmental (e.g., changes in sea temperature) stressors may have resulted in large distribution shifts in many marine fish populations (e.g., Blanchard et al., 2005; Perry et al., 2005; Pinsky et al., 2013). Most of the studies that have investigated patterns of distribution shifts have estimated changes in the centers of gravity (COGs) of fish populations directly from monitoring data (e.g., Perry et al., 2005; Dulvy et al., 2008; Pinsky et al., 2013; Engelhard et al., 2014). In other studies, spatio-temporal models were employed to compute northward and eastward COGs for understanding patterns of distribution shifts, as well as the effective area occupied of fish populations for understanding patterns of range expansion/contraction (e.g., Thorson et al., 2016a; Grüss and Thorson, 2019; Grüss et al., 2019b).

Fishing can greatly reduce the abundance of fish populations and alter their age and length structure (Li et al., 2012; Bell et al., 2015) and can have profound impacts on species interactions (Rijnsdorp et al., 2009), often resulting in the shrinkage or displacement of the spatial distribution areas of fish populations (Bell et al., 2015). Several studies found that the spatial distribution changes caused by a decline in population abundance can, in some cases,

be explained by either the proportional-density model based on ideal-free distribution theory or the basin model based on the density-dependent habitat selection theory (MacCall, 1990; Petitgas et al., 1998; Fisher and Frank, 2004; Shepherd et al., 2010; Reuchlin-Hugenholtz et al., 2015; Thorson et al., 2016b). The basin model assumes that, as the area occupied by a fish population declines as a result of a decrease in population abundance, catch rate in the areas stills occupied by the fish populations remains high (Harley et al., 2001). The assumptions of the basin model are exemplified by the collapse of the northern cod (*Gadus morhua*) fishery off eastern Canada (Walters et al., 1996; Wilberg et al., 2009). Using a spatio-temporal model, Thorson et al. (2016b) found that the basin model explained a small, yet relatively important, percentage of spatial dynamics for several groundfish stocks of the eastern Bering Sea, Gulf of Alaska, northwest Atlantic and South Africa.

Changes in the marine environment can take many forms, including profound alterations in oceanographic processes such as large fluctuations in sea temperature (Brander et al., 2003). Many studies suggest that changes in sea temperature have a great influence on fish distribution shifts, by triggering latitudinal migrations out of the areas where sea temperature becomes suboptimal, or by greatly reducing population fitness and abundance if fishes do not leave the areas where environmental conditions become suboptimal (e.g., Overholtz et al., 2011; Li et al., 2012; Cheung et al., 2013; Bell et al., 2015; Su et al., 2015). However, in a study focusing on the Atlantic mackerel (*Scomber scombrus*) population of the central Atlantic coast, Radlinski et al. (2013) found that the effect of sea temperature on fish spatial distribution varied with fish individual size and that, in some years, environmental variables other than sea temperature may have been the most important factors influencing distribution shifts. In a recent study for the eastern Bering Sea, Thorson (2019b) examined the relative impacts of local sea temperature and an annual oceanographic index (the cold pool index) in explaining the density patterns of 17 fish and invertebrate species. The authors found that

127 local sea temperature and the cold pool index jointly explained around 9-14% of the spatio-
128 temporal variation in density, and that the cold pool index explained spatio-temporal variation
129 in density in excess of local sea temperature alone.

130 The Yellow Sea is an important fishing ground located in the warm temperate zone (Fig.
131 1; Liu et al, 1990). Many fish species of high socio-economic importance inhabit the Yellow
132 Sea (Jin et al, 2005). Despite a large interest in understanding the spatio-temporal distribution
133 patterns of fish populations of the Yellow Sea in relation to environmental stressors, very few
134 studies have addressed this research issue. Many commercially important species have their
135 overwintering grounds in the Yellow Sea, including the benthopelagic small yellow croaker
136 (*Larimichthys polyactis*; hereafter referred to as "yellow croaker"). Yellow croaker is one of
137 the most representative species of the Yellow Sea (Zhu, 1963; Liu et al, 1990; Jin et al, 2005).
138 From 2001 to 2016, China's catch of yellow croaker in the Yellow and Bohai Seas has been
139 increasing, reaching 27 million tons in 2016 (Bureau of Fisheries and Fishery Administration
140 of Ministry of Agriculture, China, pers. comm.). Yellow croaker spawns in the coastal waters
141 of China, but undertakes post-spawning migrations to regions of the Yellow Sea where it is
142 also caught by South Korean fishing fleets (Jin et al., 2015). There is a critical need to better
143 understand the spatial distribution and migration patterns of yellow croaker, the changes in
144 these patterns through time, and how these patterns may respond to changes in environmental
145 stressors, to help the formulation of resource management measures for the species.

146 Yellow croaker is an economically important migratory benthopelagic fish of the Bohai,
147 Yellow and East China Seas and the western bank of the Korean Peninsula (Zhu, 1963).
148 Yellow croaker has long been targeted by Chinese, South Korean and Japanese fishing vessels
149 in the above-mentioned marine regions (Zhu, 1963). The yellow croaker population is mainly
150 divided into a northern Yellow Sea-Bohai Sea stock, a southern Yellow Sea stock, and an
151 Eastern China Sea stock (Liu et al, 1990). In the present study we analyze data for a survey

conducted in the middle and southern Yellow Sea during winter months; the area covered represents the main overwintering grounds of the northern Yellow Sea-Bohai and southern Yellow Sea stocks of yellow croaker (Liu et al, 1990; Jin et al, 2005). We refer to this area simply as the "Yellow Sea" in the remainder of the present paper. The overwintering grounds of yellow croaker in the Yellow Sea are included in those waters that are governed by the China-South Korea fisheries agreement. The fishing grounds of some of the Chinese fisheries that operate in the Yellow Sea have contracted due to the signing of this fisheries agreement. This situation has reduced the areas that Chinese fishers can fish and the amount of fish they can catch (Jin et al., 2015). The China-South Korea fisheries agreement stipulates that China is responsible for fisheries management in the western part of the Yellow Sea, and South Korea in the eastern part. Each contracting party is responsible for determining each year the allowable fishing species, fishing quota, operating time, operating area and other operating conditions of the national and foreign fishing vessels in its exclusive economic zone, and it needs to inform the other contracting party. Understanding patterns of distribution shifts and range expansion/contraction for yellow croaker in their overwintering grounds of the Yellow Sea may provide valuable information for effective resource management in the context of the China-South Korea fisheries agreement.

In the present study, we fit a delta-Gamma spatio-temporal model to bottom trawl survey biomass catch rate data for the yellow croaker population of the Yellow Sea to understand the patterns of distribution shifts and range expansion/contraction of the fish population over the period 2001-2017. We employed a spatio-temporal model rather than calculating COGs directly from monitoring data, as spatio-temporal models account for spatio-temporal changes in survey design and effort and can therefore account for random or systematic variation in sampling design when calculating changes in fish spatial distributions (Thorson et al., 2016a). First, we developed four alternative spatio-temporal models for the yellow croaker population

of the Yellow Sea, formed from a factorial cross of including or ignoring the quadratic effect of local surface temperature, as well as a spatially varying effect of the Pacific Decadal Oscillation (PDO; an annual oceanographic index), and we identified the most parsimonious of these four models based on Akaike's Information Criterion (AIC). We used the estimates of the four alternative delta-Gamma spatio-temporal models to determine the relative importance of sea temperature and the PDO in explaining spatio-temporal patterns of probability of encounter (predicted by the binomial component of the delta-Gamma model) and positive density (predicted by the Gamma component of the delta-Gamma model). Next, we employed the AIC-selected delta-Gamma spatio-temporal model to examine trends in the northward and eastwards COGs and effective area occupied of the yellow croaker population of the Yellow Sea, so as to understand patterns of distribution shifts and range expansion/contraction for the fish population. Our study uses the spatially-varying coefficient (SVC) model developed in Thorson (2019b) to represent the effects of an annual index (namely the PDO) in the spatio-temporal model of yellow croaker. This is the first time that a spatio-temporal model using the SVC model has been developed for the Yellow Sea.

2. Material and methods

2.1. Data used in this study

In this study, we used the yellow croaker biomass catch rate data ($kg.km^{-2}$) that were collected by the fixed-station bottom trawl surveys that were conducted in the Yellow Sea in the winter (January) of 2001–2011 and 2015–2017 by the Yellow Sea Fisheries Research Institute of the Chinese Academy of Fishery Sciences (Fig. 1). The research vessel "Bei Dou" (56.2-m length, 12.5-m width, 5.1-m draft, 1,165 tons and 2,250 horsepower) was employed for the surveys. Sampling consisted of 1-hour tows at a speed of 3 knots using a standard bottom trawl with 83.2 m long nets, with a 20 cm mesh, a 24 mm cod-end mesh size, and a

mouth circumference of 167.2 m. After the tows were carried out, all fishes and invertebrates were identified to species or the lowest taxonomic level possible, and abundance, biomass and biological information were then recorded for each species/taxon.

We also included sea surface temperature (SST) data for the period 2001-2017 in this study. Monthly 4 km × 4 km SST composites for January of 2001-2017 for the study area were downloaded from a National Aeronautics and Space Administration (NASA) database (http://oceandata.sci.gsfc.nasa.gov/cgi/getfile/). Remotely-sensed SST data were employed in this study, because the winter bottom trawl surveys that are conducted in the Yellow Sea do not collect any temperature data or any other environmental data. In the Yellow Sea, during the winter season, when sea temperature cools down and ocean waters mix vertically, the temperature in the water column becomes relatively uniform, so that it is reasonable to use SST as a proxy for the temperature of any layer of the water column, including the sea bottom (Jin et al., 2005; Radlinski et al., 2013). Therefore, even though yellow croaker is a benthopelagic species, it is reasonable to assume that SST has a potential relationship to its spatial distribution and density patterns during the winter season.

Finally, PDO for the period 2001-2017 were utilized in the present study. PDO estimates for 2001-2017 for the study area were downloaded from http://research.jisao.washington.edu/pdo/. We downloaded PDO estimates for December-February, from which we calculated a mean PDO value for the winter of each year of the period 2001-2017. The PDO summarizes annual variation in the location of warm waters in the North Pacific, and is the main mode of variability at a decadal time scale in the Pacific Ocean (Tian et al., 2004).

2.2. Spatio-temporal modeling

We developed four alternative delta-Gamma spatio-temporal models for the yellow croaker population of the Yellow Sea that included the effects of SST and/or the PDO or none of these effects, and we identified the most parsimonious of these four models based on AIC (Akaike, 1974). These spatio-temporal models were spatio-temporal generalized linear mixed models (GLMMs) that accounted for spatial and spatio-temporal structure at a fine scale, which were fitted to the yellow croaker biomass catch rate data collected during winter bottom trawl surveys. Specifically, we fitted the following four spatio-temporal models, which included up to 2 covariates: (1) M1: a model with no covariates; (2) M2: a model including the quadratic effect of SST, representing a dome-shaped response to local temperatures; (3) M3: a model including the spatially-varying effect of the PDO represented using an SVC model (Thorson, 2019b); and (4) M4: a model including the quadratic effect of SST and the spatially-varying effect of PDO (represented using an SVC model).

We relied on delta-Gamma GLMMs, because the yellow croaker biomass catch rate data that we employed in this study included many zeros (Thorson et al., 2015). In other words, we first fitted a binomial GLMM to encounter/non-encounter data for yellow croaker, then fitted a gamma GLMM to positive biomass catch rate data, and finally multiplied the predictions of the binomial and Gamma GLMMs to obtain final biomass-density estimates for yellow croaker (Lo et al., 1992; Grüss et al., 2019b). The spatio-temporal delta-Gamma GLMMs were implemented using R package "VAST" (Thorson, 2019a), which is publicly available online (https://github.com/James-Thorson-NOAA/VAST). We employed the spatio-temporal delta-Gamma not only to estimate spatio-temporal patterns of biomass-density for yellow croaker, but also to understand how the northward and eastward COGs and effective area occupied of the yellow croaker population may have changed over the period 2001-2017, as described in detail below. In the following, we describe the implementation of model M4

which includes the quadratic effect of SST and the spatially-varying effects of the PDO; the implementation of models M1-M3 is similar.

Yellow croaker probability of encounter p_i at site (sampling station) $s(i)$ was estimated by the binomial GLMM with a logit link function and linear predictors, including a Gaussian Markov random field representing spatial variation in probability of encounter and another Gaussian Markov random field representing spatio-temporal variation in probability of encounter:

$$p_i = logit^{-1}\left(\beta_{t(i)}^{(p)} + \omega_{s(i)}^{(p)} + \varepsilon_{s(i),t(i)}^{(p)} + \gamma_{t(i),1}^{(p)} T_{s(i),t(i)}^{(p)} + \gamma_{t(i),2}^{(p)} T_{s(i),t(i)}^{2(p)} + \xi_{s(i),t(i)}^{(p)}\right) \quad (1)$$

where $\beta_{t(i)}^{(p)}$ is the intercept for year $t(i)$ in which sample *i* was collected; $\omega_{s(i)}^{(p)}$ is the spatially correlated variability in probability of encounter at the site $s(i)$ where sample *i* was collected; $\varepsilon_{s(i),t(i)}^{(p)}$ is the spatially correlated variability in probability of encounter at site $s(i)$ in year $t(i)$; $\gamma_{t(i),1}^{(p)} T_{s(i),t(i)}^{(p)}$ is the linear effect of SST on probability of encounter at site $s(i)$ in year $t(i)$; $\gamma_{t(i),2}^{(p)} T_{s(i),t(i)}^{2(p)}$ is the quadratic effect of SST on probability of encounter at site $s(i)$ in year $t(i)$; and $\xi_{s(i),t(i)}^{(p)}$ is the spatially-varying effect of the PDO on probability of encounter at site $s(i)$ in year $t(i)$. Both the *T* and *T²* covariates were standardized to have a mean of zero and a variance of one prior to being used in the spatio-temporal models; this transformation implied that $\gamma_1^{(p)} T^{(p)}$ and $\gamma_2^{(p)} T^{2(p)}$ (i.e., *T* and *T²* times their coefficient) had a standard deviation equal to $\gamma_1^{(p)}$ and $\gamma_2^{(p)}$, respectively (Thorson, 2015; Grüss et al. 2020).

The intercept and the linear and quadratic effects of SST are fixed effects. On the other hand, the spatial term, $\omega^{(p)}$, the spatio-temporal terms, $\varepsilon_t^{(p)}$, and the spatially-varying effect of the PDO, $\xi_t^{(p)}$, are random effects and are assumed to follow a multivariate normal distribution and, in the case of the spatio-temporal terms, temporal variation is assumed to follow a random-walk process in time:

$$\omega^{(p)} \sim MVN\left(\mathbf{0}, \sigma_{p\omega}^2 \boldsymbol{R}(\kappa)\right)$$
$$\varepsilon_t^{(p)} \sim MVN\left(\varepsilon_{t-1}^{(p)}, \sigma_{p\varepsilon}^2 \boldsymbol{R}(\kappa)\right) \quad (2)$$
$$\xi_t^{(p)} \sim MVN\left(\mathbf{0}, \sigma_{p\xi}^2 \theta_s P_t\right)$$

where $\boldsymbol{R}(\kappa)$ is the correlation among locations as a function of decorrelation distance κ; $\sigma_{p\omega}^2$ is the estimated pointwise variance of the spatial variation in probability of encounter; $\sigma_{p\varepsilon}^2$ is the estimated pointwise variance of the spatio-temporal variation in probability of encounter; P_t is the PDO and $\theta_s P_t$ is the PDO effect; and $\sigma_{p\xi}^2$ is the estimated pointwise variance of the PDO effect. The $\boldsymbol{R}$ terms are calculated from a Matérn function that take geometric anisotropy (the fact that autocorrelation between locations may vary with both distance and direction) into account (Thorson et al., 2015). Following Thorson et al. (2016a), we chose to use a random-walk temporal process rather than an autoregressive process to estimate the spatio-temporal term, so as to ensure that sites and/or time intervals without sampling do not exhibit mean-reversion, which could otherwise shrink COG estimates for undersampled time periods towards the average COG for better sampled periods.

Similarly, yellow croaker positive biomass catch rate r_i at site $s(i)$ was estimated by the Gamma GLMM with a log link function and linear predictors, including a Gaussian Markov random field representing spatial variation in positive catch rate and another Gaussian Markov random field representing spatio-temporal variation in positive catch rate:

$$r_i = exp\left(\beta_{t(i)}^{(r)} + \omega_{s(i)}^{(r)} + \varepsilon_{s(i),t(i)}^{(r)} + +\gamma_{t(i),1}^{(r)} T_{s(i),t(i)}^{(r)} + \gamma_{t(i),2}^{(r)} T_{s(i),t(i)}^{2(r)} + \xi_{s(i),t(i)}^{(r)}\right) \quad (3)$$

where the parameters on the right side of Eq. (3) have the same meaning and characteristics as the parameters on the right side of Eq. (1), except that they apply to log-catch rate.

For computational efficiency, we specified 100 "knots" ($n_j = 100$) to approximate all the spatial and spatio-temporal variation terms over a fixed spatial domain Ω, such that the

value of each spatial or spatio-temporal variation term is tracked at each knot (Shelton et al., 2014). The 100 knots were uniformly distributed over a 15′ × 15′ (arc-minutes) prediction grid developed for the present study (Fig. 2). The values of all spatial and spatio-temporal variation terms are tracked at each knot by the spatio-temporal model, and the value of a spatial or spatio-temporal variation term at a given location is interpolated from the value of three knots surrounding that location (see Grüss et al. (2020) for more details about the procedure). After knots have been determined, the location of the 100 knots is held fixed when the parameters of the GLMMs are estimated. One hundred knots offered a good compromise between accuracy and computational speed; we confirmed that parameter estimates and GLMM predictions were qualitatively similar when the number of knots was increased.

After the binomial and gamma GLMMs were fitted, we mapped yellow croaker biomass-density in the Yellow Sea, using the 15′ × 15′ prediction grid developed for the present study. Next, we estimated the biomass of the yellow croaker population in year *t,* $\hat{B}_t$, as:

$$\hat{B}_t = \sum_{j=1}^{n_j} A_j \hat{p}_{j,t} \hat{r}_{j,t} \tag{4}$$

$$= \sum_{j=1}^{n_j} A_j logit^{-1}\left(\hat{\beta}_t^{(p)} + \hat{\varepsilon}_{j,t}^{(p)} + \hat{\omega}_j^{(p)} + \hat{\gamma}_{t,1}^{(p)} T_{j,t}^{(p)} + \hat{\gamma}_{t,2}^{(p)} T_{j,t}^{2(p)} + \hat{\xi}_{j,t}^{(p)}\right) exp\left(\hat{\beta}_t^{(r)} + \hat{\varepsilon}_{j,t}^{(r)} + \hat{\omega}_j^{(r)} + \hat{\gamma}_{t,1}^{(r)} T_{j,t}^{(r)} + \hat{\gamma}_{t,2}^{(r)} T_{j,t}^{2(r)} + \hat{\xi}_{j,t}^{(r)}\right)$$

where A_j is the surface area of knot *j* (in km²); $\hat{\beta}_t^{(p)}$, $\hat{\gamma}_{t,1}^{(p)}$, $\hat{\gamma}_{t,2}^{(p)}$, $\hat{\beta}_t^{(r)}$, $\hat{\gamma}_{t,1}^{(r)}$, and $\hat{\gamma}_{t,2}^{(r)}$ are fixed effects estimated through maximum likelihood estimation; and $\hat{\varepsilon}_{j,t}^{(p)}$, $\hat{\omega}_j^{(p)}$, $\hat{\xi}_{j,t}^{(p)}$, $\hat{\varepsilon}_{j,t}^{(r)}$, $\hat{\omega}_j^{(r)}$, and

$\hat{\xi}_{j,t}^{(r)}$ are random effects set to the value that maximizes the joint likelihood conditional on the estimated value of fixed effects (Thorson et al., 2015).

To understand patterns of distribution shifts for the yellow croaker population, we also estimated its eastward and northward COGs in each year of the period 2001-2017 with the spatio-temporal model. The eastward COG of yellow croaker in year *t*, X_t, is given by (Thorson et al., 2016a; Thorson and Barnett, 2017):

$$X_t = \sum_{j=1}^{n_j} x_j \frac{A_j \hat{p}_{j,t} \hat{r}_{j,t}}{\hat{B}_t} \tag{5}$$

where x_j is the value of eastings (in km) in knot j. The northward COG of yellow croaker in year *t* , Y_t, is given in a similar way, except that x_j is replaced with y_j, the value of northings (in km) in knot j, in Eq. (5).

Moreover, to understand patterns of range expansion/contraction for the yellow croaker population, we also estimated its effective area occupied in each year of the period 2001-2017 with the spatio-temporal model. Effective area occupied in year *t* is given by the ratio of estimated biomass in year *t*, $\hat{B}_t$ (given by Eq. (4)) over average biomass-density in year *t*, D_t, which is given by (Thorson et al., 2016a):

$$D_t = \sum_{j=1}^{n_j} \hat{p}_{j,t} \hat{r}_{j,t} \frac{A_j \hat{p}_{j,t} \hat{r}_{j,t}}{\hat{B}_t} \tag{6}$$

With regard to model parameter estimation, the estimation of fixed effects was accomplished by identifying the parameter values maximizing the marginal log-likelihood. First, the Laplace approximation implemented by R package "TMB" (Kristensen et al., 2016) was used to calculate the marginal log-likelihood via an approximation of the integral across all random effects. By using automatic differentiation, TMB efficiently calculates the matrix of second derivatives (which is employed by Laplace approximation), as well as the gradient

328 of the Laplace approximation (which is employed when maximizing the fixed effects).
329 Through the maximization of the marginal log-likelihood given the maximum likelihood
330 estimates of the fixed effects, TMB predicts all random effects. Additionally, for
331 computational efficiency, the probability of the random effects was approximated using the
332 stochastic partial differential equation method (Lindgren et al., 2011). The bias-correction
333 estimator developed in Thorson and Kristensen (2016) was utilized to correct for the
334 "retransformation bias" when any derived quantity involving a non-linear transformation of
335 random effects is predicted. Finally, the generalized delta method implemented in TMB was
336 employed to compute the standard errors of all fixed and random effects, as well as the
337 standard errors of derived quantities (Kass and Steffey, 1989). We confirmed that the spatio-
338 temporal model is converged by checking that the gradient of the marginal log-likelihood was
339 less than 0.0001 for all fixed effects, and that the Hessian matrix of second derivatives of the
340 negative log-likelihood was positive definite.
341
342 ***2.3. Analysis of the relative importance of SST and the PDO in explaining patterns of***
343 ***probability of encounter and positive density***
344 We took advantage of fitting four alternative spatio-temporal models (that included the
345 effects of SST and/or the PDO or none of these effects) to understand the relative importance
346 of SST and the PDO in explaining patterns of probability of encounter and positive density for
347 the yellow croaker population of the Yellow Sea. For this analysis, we implemented the
348 method used in Thorson (2015). Briefly, this method consists of comparing the estimated
349 variances of the spatio-temporal variations in probability of encounter and positive density for
350 the four alternative spatio-temporal models, so as to determine whether the inclusion of the
351 effects of SST and/or the PDO in a model leads to some reduction of the variances (Thorson,
352 2015). Here, what is meant by spatio-temporal variation is the sum of the spatial variation

term $\omega^{(p)}$ or $\omega^{(r)}$ and of the spatio-temporal variation terms $\varepsilon_t^{(p)}$ or $\varepsilon_t^{(r)}$. This spatio-temporal variation represents unmeasured (latent) variation in probability of encounter or positive density, and the desired goal of including covariates in a spatio-temporal model is to reduce this residual spatio-temporal variation as much as possible (Thorson et al., 2015).

2.4. Trend analysis of SST and PDO time series

To facilitate the interpretation of the predictions of the spatio-temporal model, we also conducted a trend analysis of SST and PDO time series. We used the regime shift detection method based on sequential *t*-test (Rodionov, 2004, 2006; Rodionov and Overland, 2005) to analyze trends in the SST and PDO environmental time series in the Yellow Sea over the period 2001-2017. The regime shift detection method based on sequential *t*-test was developed by Rodionov (2004) to detect possible regime shifts. As some of the environmental indices considered in this study may exhibit temporal autocorrelation, all environmental time series were processed with "pre-whitening" (Rodionov, 2004, 2006) before the regime shift detection method based on sequential *t*-test was implemented. The regime shift detection method based on sequential *t*-test is coded in Visual Basic and can be applied in Excel.

3. Results

3.1. Analysis of the relative importance of SST and the PDO in explaining patterns of probability of encounter and positive density

We initially developed four alternative spatio-temporal models for the yellow croaker population of the Yellow Sea (M1-M4), which included the effects of SST and/or the PDO or none of these effects. These developments allowed us to determine the relative importance of SST and the PDO in explaining patterns of probability of encounter and positive density for the yellow croaker population of the Yellow Sea. We found that SST was much more

important than the PDO in explaining patterns of probability of encounter (Table 1). Including SST in the spatio-temporal model led to a moderate reduction in the variance of spatio-temporal variation in probability of encounter, while including the PDO in the model led to a negligible reduction in the variance of spatio-temporal variation in probability of encounter. Moreover, we found that the PDO was more important than SST in explaining patterns of positive density (Table 1). Including the PDO in the spatio-temporal model resulted in a moderate decrease in the variance of spatio-temporal variation in positive density, while including SST in model led to a small increase in the variance of spatio-temporal variation in positive density.

The spatio-temporal model with no covariates (M1) had the lowest AIC (Table 2). Therefore, model M1 was selected for all subsequent analyses. We note, however, that the spatial distribution patterns, northward and eastward COGs and effective areas occupied predicted by models M1-M4 were very similar.

3.2. Patterns of spatial distribution, distribution shift and range expansion/contraction of yellow croaker in the Yellow Sea

The AIC-selected model (i.e., model M1 that did not include any covariates) predicted that, over the period 2001-2017, the highest biomass-densities of yellow croaker were found in the central area of the Yellow Sea (33°75′-36°00′N, 123°15′-124°75′E; Fig. 3). Other predicted hotspots (i.e., highest biomass-density hotspots) for yellow croaker included the north (36°00′-37°37.5′N, 123°15′-124°15′E) and southeast (32°00′-33°75′N, 124°00′-125°15′E) areas of the Yellow Sea. The spatio-temporal model also predicted that yellow croaker biomass declined markedly between 2001 and 2017, which resulted in large changes in the spatial distribution of yellow croaker in their overwintering grounds over the entire study period (Fig. 3). Since 2003, the biomass-density of yellow croaker has shown a

403 significant decrease throughout the Yellow Sea, and this decrease has been accompanied by a
404 shrinkage in high-density areas (Figs. 3 and 4). This shrinkage has been more pronounced in
405 the north and southeast areas than in the central area of the Yellow Sea. Decreases in density
406 in the southeast area was stronger after 2009/2010 than between 2001 and 2009. In 2017, the
407 central area of the Yellow Sea remained the only density hotspot for yellow croaker (Fig. 4).
408 The eastward and northward COGs estimated by the AIC-selected spatio-temporal model
409 suggest that the COG of yellow croaker moved north and west between 2001 and 2010, and
410 then south and west over the period 2010-2017 (Fig. 5). Changes in the eastward COG of
411 yellow croaker between 2001 and 2017 (i.e., the large displacement of the eastward COG of
412 the species towards the west of the Yellow Sea) were found to be significant ($p = 0.038$, using
413 a two-sided Wald test for all significance testing of changes). By contrast, changes in the
414 northward COG of yellow croaker between 2001 and 2017 were not found to be significant (p
415 > 0.05).
416 The effective area occupied estimated by the AIC-selected spatio-temporal model
417 suggests a range expansion for yellow croaker over the study period (Fig. 6). However,
418 changes in effective area occupied between 2001 and 2017 were not found to be significant (p
419 > 0.05).
420
421 ***3.3. Trend analysis of SST and PDO time series***
422 SST anomalies in the Yellow Sea were found to slightly increase between 2001 and
423 2008, markedly decline between 2008 and 2011, and largely increase between 2011 and 2017
424 (Fig. 7). The trend analysis of the SST time series suggested an absence of regime shifts in
425 SST over the period 2001-2017. The trend analysis of the PDO time series suggested that a
426 regime shift in the PDO occurred in 2013/2014 (Fig. 8). From 2001 to 2009/2010, the
427 cumulative sum of the anomaly of the PDO was usually positive. In or around 2009/2010, the

cumulative sum of the anomaly of the PDO changed from positive to negative (Fig. 8), which mirrored the switch from a southward to a northward shift in the northward COG of yellow croaker in 2009.

4. Discussion

In this study, we developed a delta-Gamma spatio-temporal model for the yellow croaker population of the Yellow Sea for the period 2001-2017. This model is one of the first spatio-temporal models for the Yellow Sea (along with Guan et al. (2019)) and the first spatio-temporal model for the Yellow Sea that implements an SVC model to represent the effects of an annual index (the PDO). The main characteristic of spatio-temporal models is the representation of spatial autocorrelation (spatial structure) to account for the fact that state variables (e.g., probability of encounter, catch rate) at given locations are more similar to state variables at nearby locations than to state variables at more distant locations. This spatial autocorrelation is modeled via spatial variation terms that represent spatial variation that is stable over time and spatio-temporal variation terms that represent spatial variation that changes between years (Grüss et al., 2017; Thorson, 2019a). The representation of spatial and spatio-temporal variation in spatio-temporal models results in more precise statistical inference and, therefore, in the delivery of more reliable scientific advice to stock and habitat assessments and resource management (Thorson et al., 2015).

Spatio-temporal models can also include covariates to improve the percentage of variability in the data explained by the spatio-temporal model (e.g., SST and the PDO in this study), or to take into account nuisance parameters (in the case of "catchability covariates"; Thorson, 2015; Grüss et al., 2020). By including the effects of SST and the PDO in the delta-Gamma spatio-temporal model of yellow croaker, we were expecting to explain as much of the spatial and spatio-temporal variations (i.e., unmeasured variations) in probability of

encounter and positive density as possible (Thorson et al., 2015). However, model selection based on AIC suggested that a model with no covariates was most parsimonious. In other words, our results suggested that neither local SST and or the regional PDO index explains a meaningful percentage of variability in the data and that, therefore, their inclusion in the delta-Gamma spatio-temporal model of the yellow croaker population of the Yellow Sea is not warranted. This result was not expected *a priori*, as previous studies for the eastern Bering Sea (Thorson, 2019b; Grüss et al., 2020) found that including sea temperature and an annual oceanographic index (the cold pool) using an SVC model led to more parsimonious spatio-temporal models capable of better describing the modeled system. We suspect that this is due to the fact that environmental variations are much more pronounced in the eastern Bering than in the Yellow Sea. Environmental variations are also less pronounced in the great majority of the world's marine regions than in the eastern Bering Sea, and the representation of spatial and spatio-temporal structure at a fine spatial scale in spatio-temporal models accounts for a large proportion of the variability in the data (Thorson et al., 2015). Therefore, we suspect that there are many regional case studies where the inclusion of environmental covariates and/or annual oceanographic indices in spatio-temporal models will not be warranted to describe the modeled system. We recommend that future studies examine this issue in several contrasted (e.g., polar, temperate and tropical) marine regions to determine if it can be generalized.

We employed the AIC-selected spatio-temporal model (i.e., the model with no covariates) to understand the spatial distribution patterns of yellow croaker in their overwintering grounds of the Yellow Sea over the period 2001-2017. The AIC-selected spatio-temporal model suggested the existence of three biomass-density hotspots (i.e., highest biomass-density areas) for yellow croaker in the Yellow Sea between 2001 and 2017: the central area of the Yellow Sea, where yellow croaker density is highest, and the north and southeast areas of the Yellow Sea. These predictions of the spatio-temporal model for the

period 2001-2017 concur with insights from a previous study that analyzed data from the 1980s (Liu et al., 1990). The analyses of Liu et al. (1990) also suggested the existence of three main overwintering grounds for yellow croaker in the Yellow Sea, specifically: (1) a northern region of the Yellow Sea located in the Chengshantou area and west of 124°00′E (Northern Yellow Sea-Bohai Sea stock); (2) a north-central region located 34°00′N-35°00′N, 123°45′E-125°00′E (Northern Yellow Sea-Bohai Sea and Central Yellow Sea stocks); and (3) a southern region located 32°00′N-34°00′N, 123°45′E-126°00′E (Southern Yellow Sea stock). The zone of the Yellow Sea where the three overwintering grounds identified in Liu et al. (1990) are connected is the central area of the Yellow Sea identified as the highest-density area for yellow croaker in the present study. The overwintering grounds of yellow croaker are important for the replenishment of the yellow croaker population, as they concentrate a large fraction of yellow croaker adults for a fraction of the year (Jin et al., 2005). Therefore, the present study provides important scientific information for spatial protection efforts that seek to preserve a fraction of yellow croaker adults to maintain its yellow croaker recruitment at reasonable levels.

We also used the AIC-selected spatio-temporal model to detect and understand patterns of distribution shifts and range/expansion for the yellow croaker population of the Yellow Sea over the period 2001-2017. Specifically, we employed the AIC-selected spatio-temporal model to estimate changes in the eastward and northward COGs and effective area occupied of the yellow croaker population. This analysis mainly suggested a statistically significant displacement of the eastward COG of yellow croaker to the west of the Yellow Sea, which reflected the progressive disappearance of yellow croaker density hotspots in the north and southeast areas of the Yellow Sea that resulted in the central area of the Yellow Sea becoming the only yellow croaker density hotspot in 2017. This finding concurs with the basin model theory, which suggests that, as the biomass of a fish population declines, biomass-density

503 becomes concentrated where habitat is most suitable (MacCall, 1990). This finding has
504 important implications for fisheries management in the context of the China-South Korea
505 fisheries agreement, as it indicates a measurable displacement of yellow croaker biomass
506 towards China.

507 Although model selection based on AIC suggested that the inclusion of SST in the
508 spatio-temporal model of yellow croaker was not warranted, we found that SST may explain a
509 moderate fraction of spatio-temporal variability in yellow croaker probability of encounter
510 (Table 1). This result concurs with the findings of previous studies that changes in sea
511 temperature may affect the spatial distribution patterns of yellow croaker in the Yellow and
512 Bohai Seas (Liu et al., 1990; Li et al., 2009; Lin et al., 2011; Chen et al., 2017; Liu et al.,
513 2017). Specifically, during the winter season, yellow croaker from the Bohai Sea and the
514 Yellow Sea coasts migrate to the wintering grounds of the Yellow Sea where high- and low-
515 salinity waters converge and warm currents allow for temperatures that are suitable for
516 wintering (Li et al., 2009; Lin et al., 2011; Chen et al., 2017; Liu et al., 2017). Previous
517 studies found that the Yellow Sea wintering grounds of yellow croaker were centered at
518 124°E prior to the 1980s, and that their location and extent were then probably affected by
519 changes in sea environmental conditions (Liu et al., 1990).

520 While model selection based on AIC suggested that the inclusion of the PDO in the
521 spatio-temporal model of yellow croaker was not warranted, we found that the PDO may
522 explain a moderate fraction of spatio-temporal variability in the positive density of yellow
523 croaker (Table 1). Further, the trend analysis of PDO time series suggested that, in 2009/2010,
524 the cumulative sum of the anomaly of the PDO changed from positive to negative, while our
525 spatio-temporal model suggested that the COG of yellow croaker started shifting northwest in
526 2009 after having shifted southwest between 2001 and 2008 (although changes in the
527 northward COG of yellow croaker between 2001 and 2017 were not found to be statistically

528 significant). Finally, the spatio-temporal model predicted that the declines in yellow croaker
529 density that occurred in the southeast area of the Yellow Sea were stronger between
530 2009/2010 and 2017 than between 2001 and 2009. Therefore, we conclude that changes in the
531 PDO towards the end of the study period (switching from a positive to a negative phase) may
532 have synergistically interacted with biomass declines in making the yellow croaker density
533 hotspot of the southeast area of the Yellow Sea disappear. This result shows the potential,
534 although moderate, for large-scale oceanographic events in the Pacific to contribute to fish
535 distribution shifts in the Yellow Sea. This kind of information is important for resource
536 managers, as it offers them the possibility to anticipate potential distribution shifts in response
537 to changes in large-scale oceanographic indices, and to craft management measures
538 accordingly (Karp et al., 2019).
539 Fishing pressure can also contribute to patterns of distribution shifts and range
540 expansion/contraction in fish populations (Bell et al., 2015). In particular, fishing pressure
541 was identified as a primary driving force behind distribution shifts in the Yellow and Bohai
542 Seas in some previous studies (Xu et al., 2003; Wang et al., 2012; Lin et al., 2016). For this
543 reason, we initially fitted spatio-temporal models that also included the effect of fishing
544 power (a proxy for fishing pressure), which was modeled as an annual index using the SVC
545 model (Results not shown). However, we found that fishing pressure had virtually no effect
546 on the probability of encounter and positive density of yellow croaker in the Yellow Sea. We
547 were not expecting this result *a priori*, as Xu et al, (2003) and Li (2011) both reported that
548 fishing pressure is unevenly distributed in the Yellow Sea, and is higher in the central and
549 southern parts of the Yellow Sea than in the northern Yellow Sea. Li (2011) also found that
550 the density of yellow croaker was lower in the southern than in the northern Yellow Sea over
551 the period 1999-2010, due to the differing spatial patterns of fishing pressure in the northern
552 and southern Yellow Sea and also, to a lesser extent, to the increase in SST that occurred in

553 the southern Yellow Sea between 1999 and 2010. Li (2011)'s findings may explain why our
554 spatio-temporal model predicted that the effective area occupied of yellow croaker slightly
555 contracted along the north-south axis with a small displacement of its southern population
556 boundary to the north (Fig. 4). Fishing power (specifically the logarithm of the mean power of
557 the fishing boats from the four northern provinces of China and the city of Tianjing) was the
558 only fishing pressure indicator available to us, but may be far from the best way to describe
559 fishing pressure in a spatio-temporal model. Therefore, we recommend that future studies
560 obtain more meaningful indicators of fishing pressure to re-examine the relative importance
561 of fishing pressure in explaining patterns of probability of encounter and positive density for
562 yellow croaker with spatio-temporal models.
563 We also encourage future studies to investigate whether patterns of distribution shifts
564 and range expansion/contraction for yellow croaker vary among length classes. Length data
565 are available for yellow croaker for a fraction of the stations sampled in the Yellow Sea.
566 When considering the entire population of Atlantic mackerel (*Scomber scombrus*) of the
567 central Atlantic coast (i.e., all length classes combined), Radlinski et al. (2013) found no
568 significant correlation between Atlantic mackerel spatial distribution patterns and SST
569 anomality. However, when the Atlantic mackerel population was divided into three length
570 groups, the authors found a significant correlation between the spatial distribution patterns of
571 >33-cm mackerels and SST anomaly. Similarly, we suspect that some length groups of the
572 yellow croaker population of the Yellow Sea may be more sensitive to changes in
573 environmental indices than others; therefore, we recommend that future studies develop
574 spatio-temporal models for different length groups of yellow croaker and examine the relative
575 importance of SST and the PDO in explaining patterns of distribution shifts and range
576 expansion/contraction for these length groups. It would then be possible for future resource
577 management efforts in the Yellow Sea to craft spatial protection plans for specific length

groups (e.g., juvenile or adult fishes) in relation to past and anticipated environmental and fishing patterns (Grüss et al., 2018, 2019a).

In the present study, we considered four alternative delta-Gamma spatio-temporal models that included the effects of covariates (SST and/or the PDO) on both probability of encounter and positive density or none of these effects. Yet, previous studies that employed delta models found that a covariate that had a significant effect on probability of encounter did not necessarily have a significant effect on positive density, or vice versa (e.g., Vaz et al., 2006; Grüss et al., 2014; Weijerman et al., 2019). Thus, in this study, we could have considered some additional alternative delta-Gamma spatio-temporal models that included the effects of covariates on either probability of encounter or positive density (Grüss et al., 2020). However, we found that the spatial distribution patterns, northward and eastward COGs and effective areas occupied predicted by the four alternative models fitted in this study were very similar. Therefore, we suspect that, had we fitted additional models, the model with no covariates would have still been selected based on AIC and the findings of this study would have been unaltered. That said, we encourage future studies using our spatio-temporal modeling framework for the Yellow Sea to consider additional models including the effects of covariates on either probability of encounter or positive density.

The present study provides important information for the resource management efforts that target yellow croaker in their overwintering grounds of the Yellow Sea. It also provides a spatio-temporal modeling framework for carrying research investigations for the other species that inhabit the Yellow Sea. Importantly, our spatio-temporal modeling framework will allow fisheries managers to assess the potential impacts of distribution shifts and range expansion/contraction for socio-economically important species on the catches of Chinese fishing vessels, in the context of the China-South Korea fisheries agreement. Our spatio-temporal modeling framework will also contribute valuable information about essential fish

habitats (e.g., spawning and nursery grounds) and their spatial evolution through time, thereby supporting the development of spatial protection plans and other resource management measures for the Yellow Sea.

Authorship statement

QH, AG and JTT designed and analyzed the models; QH and AG conceived the models; XS and XJ had a role in study design and data collection; all authors wrote the paper; all authors have approved the final article.

Acknowledgments

We thank very much the members of the Division of Fishery Resources and Ecosystem of the Yellow Sea Fisheries Research Institute, the Chinese Academy of Fishery Sciences, and the crew of R/V *"Bei Dou"* for having collected the survey data used in this study. Many thanks as well to two NOAA internal reviewers (Lee Qi and Jason Conner) for their insightful comments on an early version of the manuscript. The scientific results and conclusions, as well as any views or opinions expressed herein, are those of the authors and do not necessarily reflect those of NOAA or the U.S. Department of Commerce. All authors have no conflicts of interest to declare.

References

Akaike, H., 1974. A new look at statistical-model identification. IEEE Transactions on Automatic Control 19, 716−723.

Bell, R.J., Richardson, D.E., Hare, J.A., Lynch, P.D., Fratantoni, P.S., 2015. Disentangling the effects of climate, abundance, and size on the distribution of marine fish: an example based on four stocks from the northeast us shelf. ICES Journal of Marine Science 72(5), 1311-1322.

Blanchard, J.L., Mills, C., Jennings, S., Fox, C.J., Rackham, B.D., Eastwood, P.D., O'Brien, C.M., 2005. Distribution abundance relationships for North Sea Atlantic cod (*Gadus morhua*): observation versus theory. Canadian Journal of Fisheries and Aquatic Sciences 62(9), 2001-2009.

633 Brander, K.M., Blom, G., Borges, M.F., Erzini, K., Henderson, G., MacKenzie, B.R.,
634 Mendes, H., Ribeiro, J., Santos, A.M.P., Toresen, R., 2003. Changes in fish distribution in
635 the eastern North Atlantic: Are we seeing a coherent response to changing temperature?
636 ICES Marine Science Symposia 219, 261-270.
637 Chen, Y.L., Shan, X.J., Jin, X.S., Johannessen, A., Yang, T., Dai, F.Q., 2017. Changes in fish
638 diversity and community structure in the central and southern yellow sea from 2003 to
639 2015. Chinese Journal of Oceanology and Limnology 36(2), 1-13.
640 Cheung, W.W.L., Lam, V.W.Y., Sarmiento, J.L., Kearney, K., Watson, R., Pauly, D., 2009.
641 Projecting global marine biodiversity impacts under climate change scenarios. Fish and
642 Fisheries 10(3), 235-251.
643 Cheung, W.W.L., Pinnegar, J., Merino, G., Jones, M.C., Barange, M., 2012. Review of
644 climate change impacts on marine fisheries in the UK and Ireland. Aquatic Conservation:
645 Marine and Freshwater Ecosystems 22(3), 368-388.
646 Cheung, W.W.L., Watson, R., Pauly, D., 2013. Signature of ocean warming in global fisheries
647 catch. Nature 497(7449), 365-368.
648 Dulvy, N.K., Rogers, S.I., Jennings, S., Stelzenmuller. V., Dye, S.R., Skjoldal, H.R., 2008.
649 Climate change and deepening of the North Sea fish assemblage: a biotic indicator of
650 warming seas. Journal of Applied Ecology 45(4), 1029–1039.
651 Engelhard, G.H., Righton, D.A., Pinnegar, J.K., 2014. Climate change and fishing: a century
652 of shifting distribution in North Sea cod. Global Change Biology 20(8), 2473–2483.
653 Fisher, J., Frank, K.T., 2004. Abundance-distribution relationships and conservation of
654 exploited marine fishes. Marine Ecology Progress 279(1), 201-213.
655 Grüss, A., Biggs, C., Heyman, W.D., Erisman, B., 2018. Prioritizing monitoring and
656 conservation efforts for fish spawning aggregations in the U.S. Gulf of Mexico.
657 Scientific Reports, 8, 8473.
658 Grüss, A., Biggs. C.R., Heyman, W.D., Erisman, B., 2019a. Protecting juveniles, spawners or
659 both: A practical statistical modelling approach for the design of marine protected areas.
660 Journal of Applied Ecology 56(10), 2328-2339.
661 Grüss, A., Drexler, M., Ainsworth, C. H., 2014. Using delta generalized additive models to
662 produce distribution maps for spatially explicit ecosystem models. Fisheries Research,
663 159, 11-24.
664 Grüss, A., Gao, J., Thorson, J.T., Rooper, C.N., Thompson, G., Boldt, J.L., Lauth, R., 2020.
665 Estimating synchronous changes in condition and density in eastern Bering Sea fishes.
666 Marine Ecology Progress Series, 635, 169-185.
667 Grüss, A., Thorson, J.T., 2019. Developing spatio-temporal models using multiple data types
668 for evaluating population trends and habitat usage. ICES Journal of Marine Science
669 76(6), 1748-1761.
670 Grüss, A., Thorson, J.T., Sagarese, S.R., Babcock, E.A., Karnauskas, M., Walter, J.F.,
671 Drexler, M., 2017. Ontogenetic spatial distributions of red grouper (*Epinephelus morio*)
672 and gag grouper (*Mycteroperca microlepis*) in the US Gulf of Mexico. Fisheries
673 Research 193, 129–142.
674 Grüss A., Walter III J.F., Babcock E.A., Forrestal F.C., Thorson J.T., Lauretta M.V., Schirripa
675 M.J., 2019b. Evaluation of the impacts of different treatments of spatio-temporal
676 variation in catch-per-unit-effort standardization models. Fisheries Research 213, 75-93.
677 Guan, L., Jin, X., Wu, Q., Shan, X., 2019. Statistical modelling for exploring diel vertical
678 movements and spatial correlations of marine fish species: a supplementary tool to assess
679 species interactions. ICES Journal of Marine Science, 76(6), 1776-1783.
680 Harley, S.J., Myers, R.A., Dunn, A., 2001. Is catch-per-unit-effort proportional to abundance?
681 Canadian Journal of Fisheries and Aquatic Sciences 58(9), 1760-1772.

682 Jin, X.S., Dou, S.Z., Shan, X.J., Wang, Z.Y., Wan, R.J., Bian, X.D., 2015. Hot spots of
683 frontiers in the research of sustainable yield of Chinese inshore fishery. Progress in
684 Fishery Sciences 36 (1), 124-131 (in Chinese).
685 Jin, X.S., Zhao, X.Y., Meng, T.X., Cui, Y., 2005. Biological Resource and Habitation
686 Environment of the Bohai and Yellow Sea. Science Press 241-261 (in Chinese).
687 Karp, M.A., Peterson, J.O., Lynch, P.D., Griffis, R.B., Adams, C.F., Arnold, W.S., Barnett,
688 L.A.K., deReynier, Y., DiCosimo, J., Fenske, K.H., Gaichas, S.K., Hollowed, A.,
689 Holsman, K., Karnauskas, M., Kobayashi, D., Leising, A., Manderson, J.P., McClure,
690 M., Morrison, W.E., Schnettler, E., Thompson, A., Thorson, J.T., Walter III, J.F., Yau,
691 A.J., Methot, R.D., Link, J.S., 2019. Accounting for shifting distributions and changing
692 productivity in the development of scientific advice for fishery management. ICES
693 Journal of Marine Science 76 (5), 1305–1315.
694 Kass, R.E., Steffey, D., 1989. Approximate Bayesian inference in conditionally independent
695 hierarchical models (parametric empirical Bayes models). Journal of the American
696 Statistical Association 84, 717–726.
697 Kristensen, K., Nielsen, A., Berg, C.W., Skaug, H., Bell, B., 2016. TMB: Automatic
698 Differentiation and Laplace Approximation. Journal of Statistical Software 70(5), 1–21.
699 Li, Z.L., 2011. Interannual changes in biological characteristics of small yellow croaker
700 *Larimichthys polyactis*, Pacific cod *Gadus macrocephalus* and anglerfish *Lophius litulon*
701 in the Bohai Sea and Yellow Sea. Qingdao: The Institute of Oceanology, Chinese
702 Academy of Sciences 40-55 (in Chinese).
703 Li, J.S., Lin, L.S., Cheng, J.H., 2009. Distribution characteristic of small yellow croaker
704 (*Larimichthys polyactis Bleeker*) and its relationship with bottom water temperature and
705 salinity in the northern East China Sea in autumn. Journal of Fishery Sciences of China
706 16(3), 348-356 (in Chinese).
707 Li, Z.L., Jin, X.S., Zhang, B., Zhou, Z.P., Shan, X.J., Dai, F.Q., 2012. Interannual variations
708 in the population characteristics of the Pacific cod *Gadus macrocephalus* in the Yellow
709 Sea. Oceanologia et Limnologia Sinica 43(5), 924-931 (in Chinese).
710 Lin, Q., Wang, J., Yuan, W., Fan, Z.H., Jin, X.S., 2016. Effects of fishing and environmental
711 change on the ecosystem of the Bohai Sea. Journal of Fishery Sciences of China 23(3),
712 619-629 (in Chinese).
713 Lin, X., Yang, J., Guo, J., Zhang, Z., Yin, Y., Song, X., 2011. An asymmetric upwind flow,
714 Yellow Sea Warm Current: 1. New observations in the western Yellow Sea. Journal of
715 Geophysical Research Atmospheres 116(C4), 0148-0227C04026.
716 Lindgren, F., Rue, H., Lindström, J., 2011. An explicit link between Gaussian fields and
717 Gaussian Markov random fields: The stochastic partial differential equation approach.
718 Journal of the Royal Statistical Society: Series B (Statistical Methodology) 73(4), 423–
719 498.
720 Liu, X.X., Wang, J., Xu, B.D., Xue, Y., Ren, Y.P., 2017. Impacts of fishing pressure and
721 climate change on catches of small yellow croaker in the Yellow Sea and Bohai Sea.
722 Periodical of Ocean University of China 47(8), 58-64 (in Chinese).
723 Liu, X.S., Wu, J.N., Han, G.Z., Lin, J.Q., Lin, F.S., Yao, Y.M., 1990. Fishery resources
724 investigation and regionalization District in the Bohai Sea and the Yellow Sea. China
725 Ocean Press, Beijing, China (in Chinese).
726 Lo, N.C., Jacobson, L.D., Squire, J.L., 1992. Indices of relative abundance from fish spotter
727 data based on delta-lognornial models. Canadian Journal of Fisheries and Aquatic
728 Sciences 49(12), 2515-2526.
729 MacCall, A.D., 1990. Dynamic Geography of Marine Fish Populations. Washington Sea
730 Grant Program, University of Washington Press, Seattle, WA (153 p).

Overholtz, W.J., Hare, J.A., Keith, C.M., 2011. Impacts of Interannual Environmental Forcing and Climate Change on the Distribution of Atlantic Mackerel on the U.S. Northeast Continental Shelf. Marine and Coastal Fisheries 3(1), 219-232.

Perry, A.L., Low, P.J., Ellis, J.R., Reynolds, J.D., 2005. Climate Change and Distribution Shifts in Marine Fishes. Science 308(5730), 1912-1915.

Petitgas, P., 1998. Biomass-dependent dynamics of fish spatial distributions characterized by geostatistical aggregation curves. ICES Journal of Marine Science 55(3), 443-453.

Pinsky, M.L., Worm, B., Fogarty, M.J., Sarmiento, J.L., Levin, S.A., 2013. Marine taxa track local climate velocities. Science 341(6151), 1239-1242.

Radlinski, M.K., Sundermeyer, M.A., Bisagni, J.J., 2013. Spatial and temporal distribution of Atlantic mackerel (*Scomber scombrus*) along the northeast coast of the United States, 1985–1999. ICES Journal of Marine Science 70(6), 1151-1161.

Reuchlin-Hugenholtz, E., Shackell, N.L., Hutchings, J.A., Stergiou, K.I., 2015. The potential for spatial distribution indices to signal thresholds in marine fish biomass. PLOS ONE 10(3), e0120500.

Rijnsdorp, A., Peck, M., Engelhard, G., Mllmann, C., Pinnegar, J., 2009. Resolving the effect of climate change on fish populations. ICES Journal of Marine Science 66, 1570–1583.

Rodionov, S.N., 2004. A sequential algorithm for testing climate regime shifts. Geophysical Research Letters 31(9), L09204.

Rodionov, S.N., 2006. The use of prewhitening in climate regime shift detection, Geophys. Geophysical Research Letters 33(12), L12707.

Rodionov, S., Overland, J.E., 2005. Application of a sequential regime shift detection method to the Bering Sea ecosystem. ICES Journal of Marine Science 62(3), 328-332.

Shelton, A.O., Thorson, J.T., Ward, E.J., Feist, B.E., 2014. Spatial semiparametric models improve estimates of species abundance and distribution. Canadian Journal of Fisheries and Aquatic Sciences 71(11), 1655-1666.

Shepherd, T.D., Litvak, M.K., 2010. Density-dependent habitat selection and the ideal free distribution in marine fish spatial dynamics: considerations and cautions. Fish and Fisheries 5(2), 141-152.

Su, H., Chen, X.J., Wang, J.T., 2015. Influence of sea surface temperature changes on Scomber japonicas habitat in the Yellow Sea and East China Sea. Acta Oceanologica Sinica 37 (6), 88-96 (in Chinese).

Thorson, J.T., 2015. Spatio-temporal variation in fish condition is not consistently explained by density, temperature, or season for California Current groundfishes. Marine Ecology Progress Serires 526, 101–112.

Thorson, J.T., 2019a. Guidance for decisions using the Vector Autoregressive Spatio-Temporal (VAST) package in stock, ecosystem, habitat and climate assessments. Fisheries Research 210, 143–161.

Thorson, J.T., 2019b. Measuring the impact of oceanographic indices on species distribution shifts: The spatially varying effect of cold-pool extent in the eastern Bering Sea. Limnology and Oceanography 64(6), 2632-2645.

Thorson, J.T., Barnett, L.A.K., 2017. Comparing estimates of abundance trends and distribution shifts using single- and multispecies models of fishes and biogenic habitat. ICES Journal of Marine Science 74, 1311–1321.

Thorson, J.T., Kristensen, K., 2016. Implementing a generic method for bias correction in statistical models using random effects, with spatial and population dynamics examples. Fisheries Research 175, 66–74.

Thorson, J.T., Pinsky, M.L., Ward, E.J., 2016a. Model-based inference for estimating shifts in species distribution, area occupied and centre of gravity. Methods in Ecology and Evolution 7(8), 990-1002.

781 Thorson, J.T., Rindorf, A., Gao, J., Hanselman, D.H., Winker, H., 2016b. Density-dependent
782 changes in effective area occupied for sea-bottom-associated marine fishes. Proceedings
783 of the Royal Society B: Biological Sciences 283(1840), 20161853.
784 Thorson, J.T., Shelton, A.O., Ward, E.J., Skaug, H.J., 2015. Geostatistical delta-generalized
785 linear mixed models improve precision for estimated abundance indices for west coast
786 groundfishes. ICES Journal of Marine Science 72(5), 1297-1310.
787 Tian, Y., Ueno, Y., Suda, M., Akamine., T. 2004. Decadal variability in the abundance of
788 Pacific saury and its response to climatic/oceanic regime shifts in the northwestern
789 subtropical Pacific during the last half century. Journal of Marine Systems, 52(1-4), 235-
790 257.
791 Vaz, S., Pavoine, S., Koubbi, P., Loots, C., Coppin, F., 2006. Spatiotemporal characteristics
792 of fish populations in relation to environmental forcing functions as a component of
793 ecosystem-based assessment: effects on catchability. ICES CM 2006/O: 06.
794 Walters, C., Maguire, J. J., 1996. Lessons for stock assessment from the northern cod
795 collapse. Reviews in Fish Biology and Fisheries 6(2), 125-137.
796 Wang, Y.Z., Sun, D.R., Lin, Z.J., Wang, X.H., Jia, X.P., 2012. Analysis on responses of
797 hairtail catches to fishing and climate factors in the Yellow Sea and Bohai Sea, China.
798 Journal of Fishery Sciences of China 19(6), 1043-1050 (in Chinese).
799 Weijerman, M., Grüss, A., Dove, D., Asher, J., Williams, I. D., Kelley, C., Drazen, J. C.,
800 2019. Shining a light on the composition and distribution patterns of mesophotic and
801 subphotic fish communities in Hawai ‘i. Marine Ecology Progress Series, 630, 161-182.
802 Wilberg, M.J., Thorson, J.T., Linton, B.C., Berkson, J., 2009. Incorporating time-varying
803 catchability into population dynamic stock assessment models. Reviews in Fisheries
804 Science 18(1), 7-24.
805 Xu, B.D., Jin, X.S., Liang, Z.L., 2003. Changes of demersal fish community structure in the
806 Yellow Sea during the autumn. Journal of Fishery Sciences of China 10(2):148-154 (in
807 Chinese).
808 Zhu, Y.D., 1963. Study on the classification of sciaenid fishes in China and description of
809 new genus and species. Shanghai Scientific and Technical Publishers, Shanghai, China
810 (in Chinese).
811 http://oceandata.sci.gsfc.nasa.gov/cgi/getfile/
812 http://research.jisao.washington.edu/pdo/
813 https://github.com/James-Thorson-NOAA/VAST

814 **Figure captions**

815 **Fig. 1. Map of the study area showing the spatial distribution of the bottom trawl survey**
816 **stations where the biomass catch rate data used in this study were collected.**

817

818 **Fig. 2. Location of the barycenter of extrapolation grid cells and of "knots" in the study**
819 **area**. A 15′ × 15′ (arc-minutes) extrapolation grid was constructed for the present study to
820 allow for the production of maps. This extrapolation grid includes 272 cells, whose
821 barycenters are shown in **(a, b)**. For computational efficiency, 100 "knots" were specified to
822 approximate the spatial and spatio-temporal variation terms of the spatio-temporal model
823 developed in this study; these knots are shown in **(c)**.

824

825 **Fig. 3. Spatial patterns of log-density for the small yellow croaker (*Larimichthys***
826 ***polyactis*) population of the Yellow Sea in each year of the period 2001-2017, predicted**
827 **by the Akaike's information criterion-selected spatio-temporal model developed for the**
828 **fish population.** The color legend is provided in the first panel and has units ln(kg.km^{-2}).
829 Only predictions for those years where biomass trawl survey data were available for small
830 yellow croaker (i.e., 2001–2011 and 2015–2017) are shown.

831

832 **Fig. 4. Similar to Fig.3, except that spatial patterns of log-density in each year of the**
833 **period 2001-2017 are shown only for those areas where log-density is greater than 1% of**
834 **the maximum expected log-density over the entire study period.** For each year of the
835 period 2001-2017, the areas where log-density is less than 1% of the maximum expected log-
836 density over the entire study period are highlighted in light grey.

837

838 **Fig. 5. Eastward center of gravity (COG; in km) and northward COG (in km) of the**
839 **small yellow croaker (*Larimichthys polyactis*) population of the Yellow Sea in each year**
840 **of the period 2001-2017, predicted by the Akaike's information criterion-selected spatio-**
841 **temporal model developed for the fish population.** For both panels, the shaded areas
842 represent 95% confidence intervals. Only predictions for those years where biomass trawl
843 survey data were available for small yellow croaker (i.e., 2001–2011 and 2015–2017) are
844 shown.
845
846 **Fig. 6. Effective area occupied (in ln(km²)) of the small yellow croaker (*Larimichthys**
847 ***polyactis*) population of the Yellow Sea in each year of the period 2001-2017, predicted**
848 **by the Akaike's information criterion-selected spatio-temporal model developed for the**
849 **fish population.** The shaded areas represent 95% confidence intervals. Only predictions for
850 those years where biomass trawl survey data were available for small yellow croaker (i.e.,
851 2001–2011 and 2015–2017) are shown.
852
853 **Fig. 7. Changes in winter sea surface temperature anomalies (SSTA, in °C) in the Yellow**
854 **Sea over the period 2001-2017.**
855
856 **Fig. 8. Pacific Decadal Oscillation (PDO) anomaly (red bars), as well as the cumulative**
857 **sum of the PDO anomalies (orange line), in the Yellow Sea during the winter season, in**
858 **each year of the period 2001-2017.** The regime shift in the PDO revealed using the regime
859 shift detection method based on sequential *t*-test is also shown here (blue line).

Tables

Table 1. Comparison of the variances of the spatio-temporal variations in probability of encounter and positive density estimated by the four alternative delta-Gamma spatio-temporal models developed in this study (M1-M4). Here, spatio-temporal variation in probability of encounter refers to the sum of the spatial and spatio-temporal variation terms estimated by the binomial component of the delta-Gamma spatio-temporal model, and spatio-temporal variation in positive density refers to the sum of the spatial and spatio-temporal variation terms estimated by the Gamma component of the spatio-temporal model. % change in variance = Percent change in variance compared to model M1 that does not include any covariates; SST = sea surface temperature; PDO = Pacific Decadal Oscillation.

Model (covariates included)	Variance for the binomial component of the model	% change in variance for the binomial component	Variance for the Gamma component of the model	% change in variance for the Gamma component
M1 (None)	0.0161	-	0.1170	-
M2 (SST)	0.0127	- 26.7 %	0.1316	+ 11.1 %
M3 (PDO)	0.0162	+ 0.4 %	0.0988	- 18.4 %
M4 (SST + PDO)	0.0128	- 26.2 %	0.1149	- 1.9 %

871 **Table 2.** Model selection results using Akaike's information criterion (AIC) applied to the
872 maximum marginal likelihood for each of the four alternative delta-Gamma spatio-temporal
873 models fitted in this study. SST = sea surface temperature; PDO = Pacific Decadal
874 Oscillation.

Model	Covariates	ΔAIC
M1	None	0
M2	SST	4.251
M3	PDO	3.772
M4	SST + PDO	8.147

875

876 **Fig. 1**

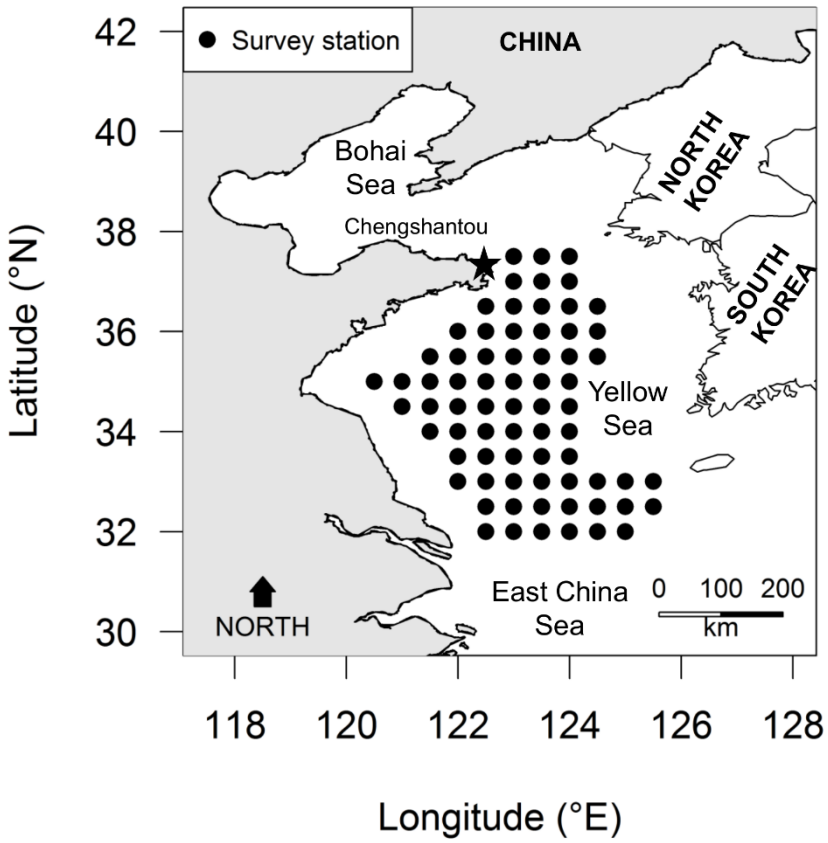
Survey station
CHINA
Bohai Sea
Chengshantou
NORTH KOREA
SOUTH KOREA
Yellow Sea
East China Sea
NORTH
0 100 200
km
Latitude (°N)
Longitude (°E)
42
40
38
36
34
32
30
118
120
122
124
126
128

877 **Fig. 2**

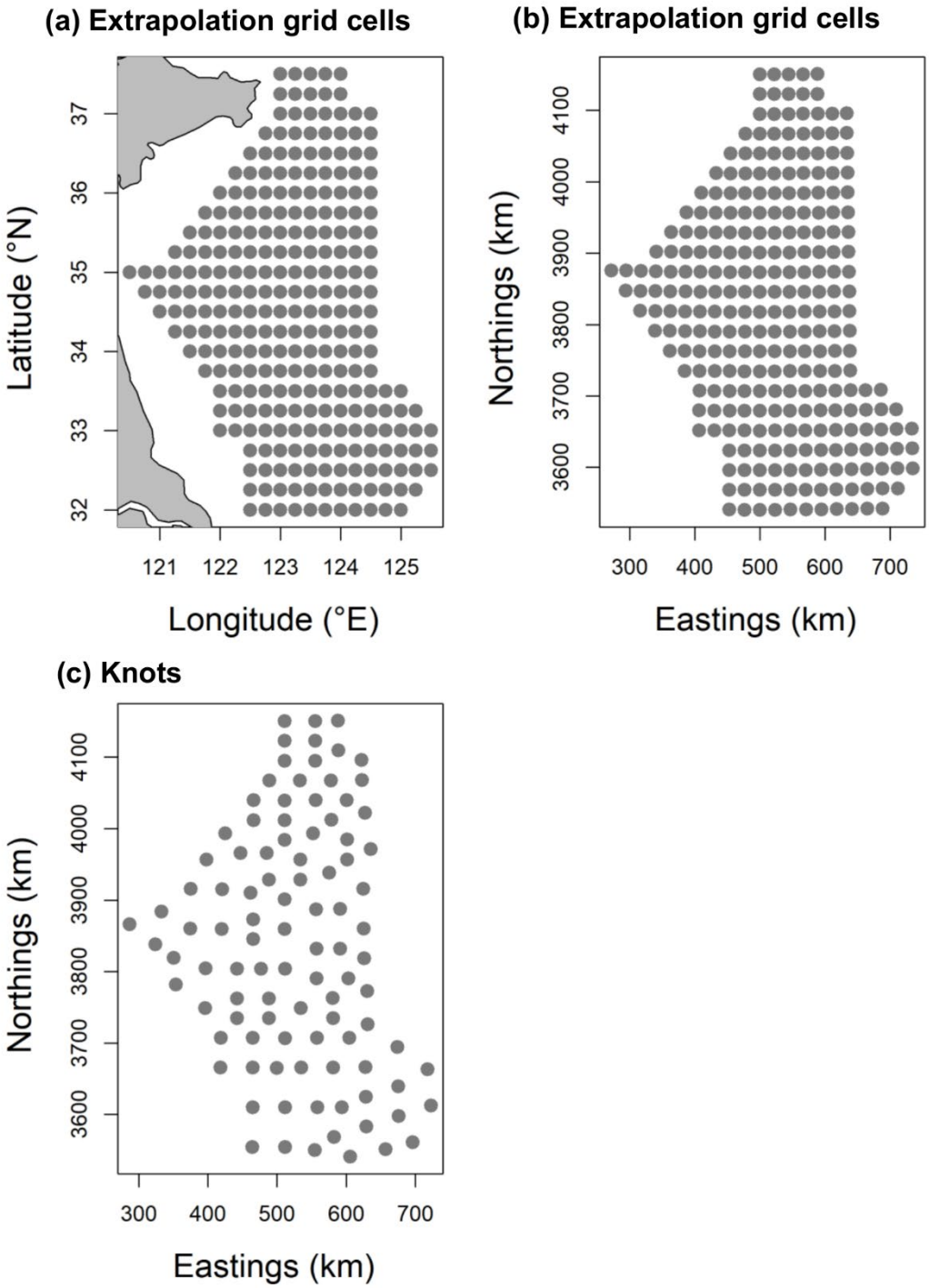
(a) Extrapolation grid cells
Latitude (°N)
32
33
34
35
36
37
121
122
123
124
125
Longitude (°E)
(b) Extrapolation grid cells
Northings (km)
3600
3700
3800
3900
4000
4100
300
400
500
600
700
Eastings (km)
(c) Knots
Northings (km)
3600
3700
3800
3900
4000
4100
300
400
500
600
700
Eastings (km)

878 **Fig. 3**

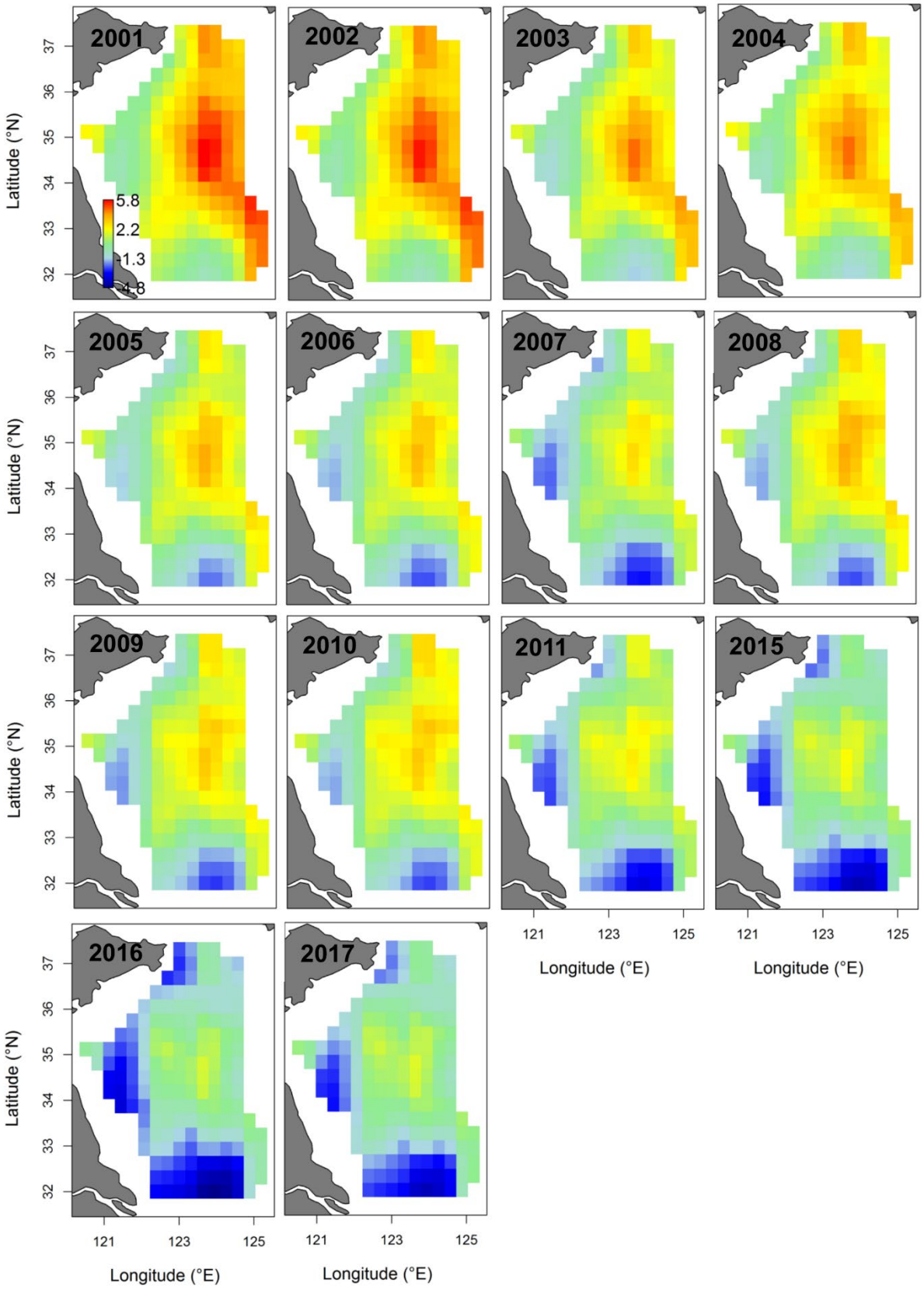
2001
2002
2003
2004
2005
2006
2007
2008
2009
2010
2011
2015
2016
2017
5.8
2.2
1.3
0.8
Latitude (°N)
32
33
34
35
36
37
121
123
125
Longitude (°E)

879 **Fig. 4**

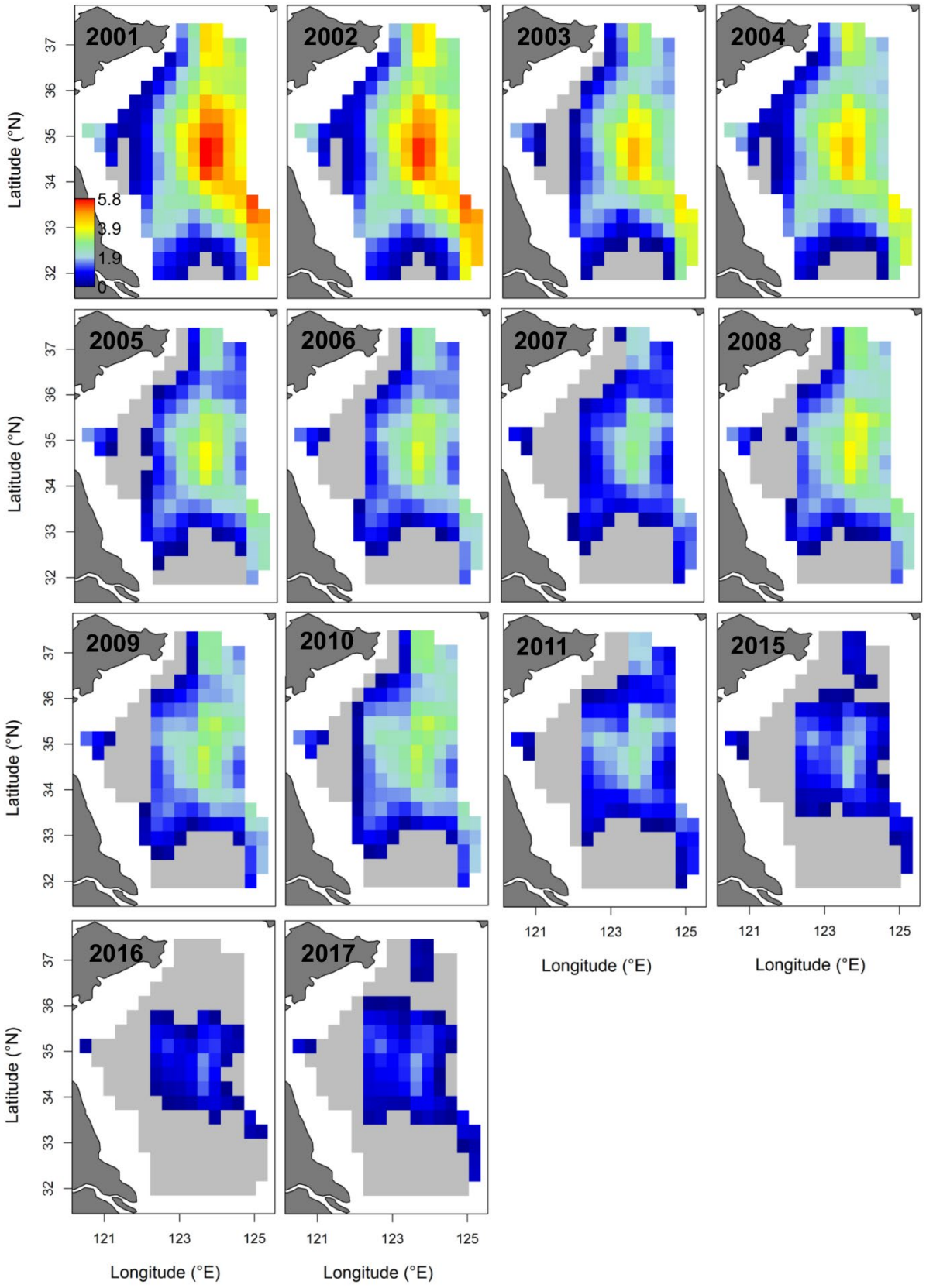
2001
2002
2003
2004
2005
2006
2007
2008
2009
2010
2011
2015
2016
2017
5.8
3.9
1.9
0
Latitude (°N)
Longitude (°E)
32
33
34
35
36
37
121
123
125

880 **Fig. 5**

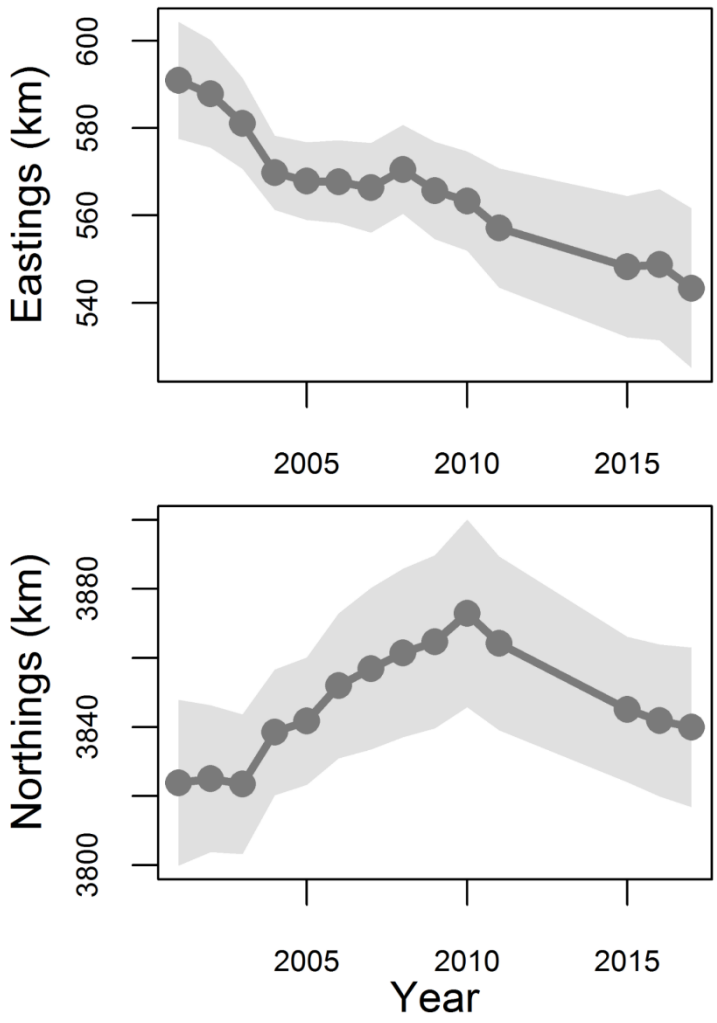
Eastings (km)
540
560
580
600
2005
2010
2015
Northings (km)
3800
3840
3880
2005
2010
2015
Year

881 **Fig. 6**

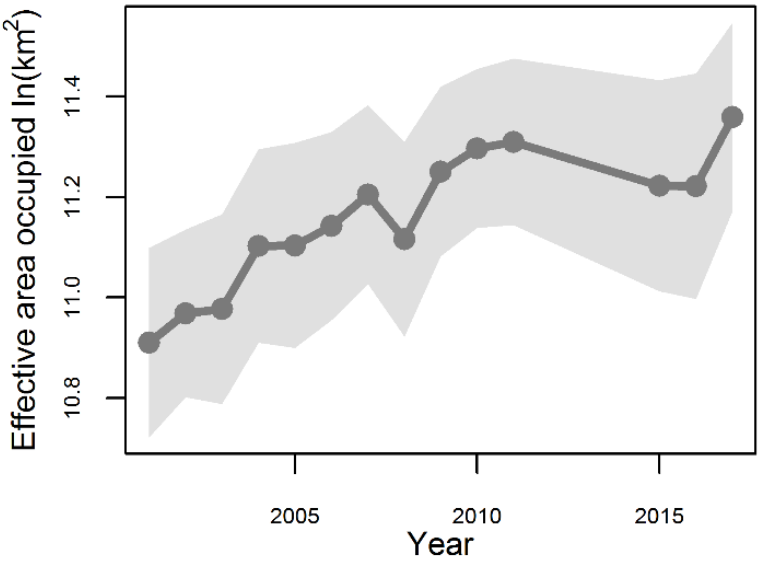
Effective area occupied ln(km^2)
10.8
11.0
11.2
11.4
2005
2010
2015
Year

882 **Fig. 7**

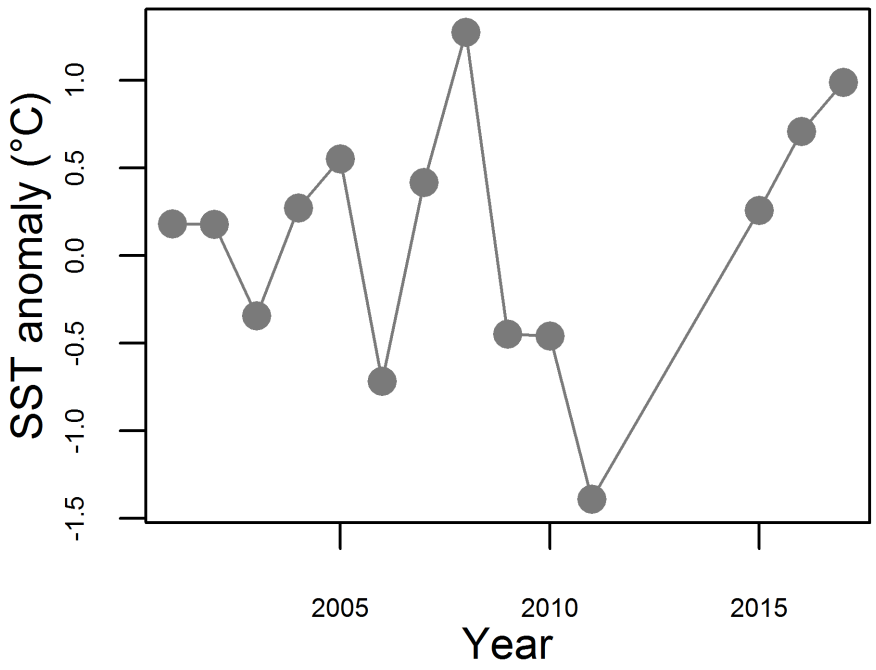

883 **Fig. 8**

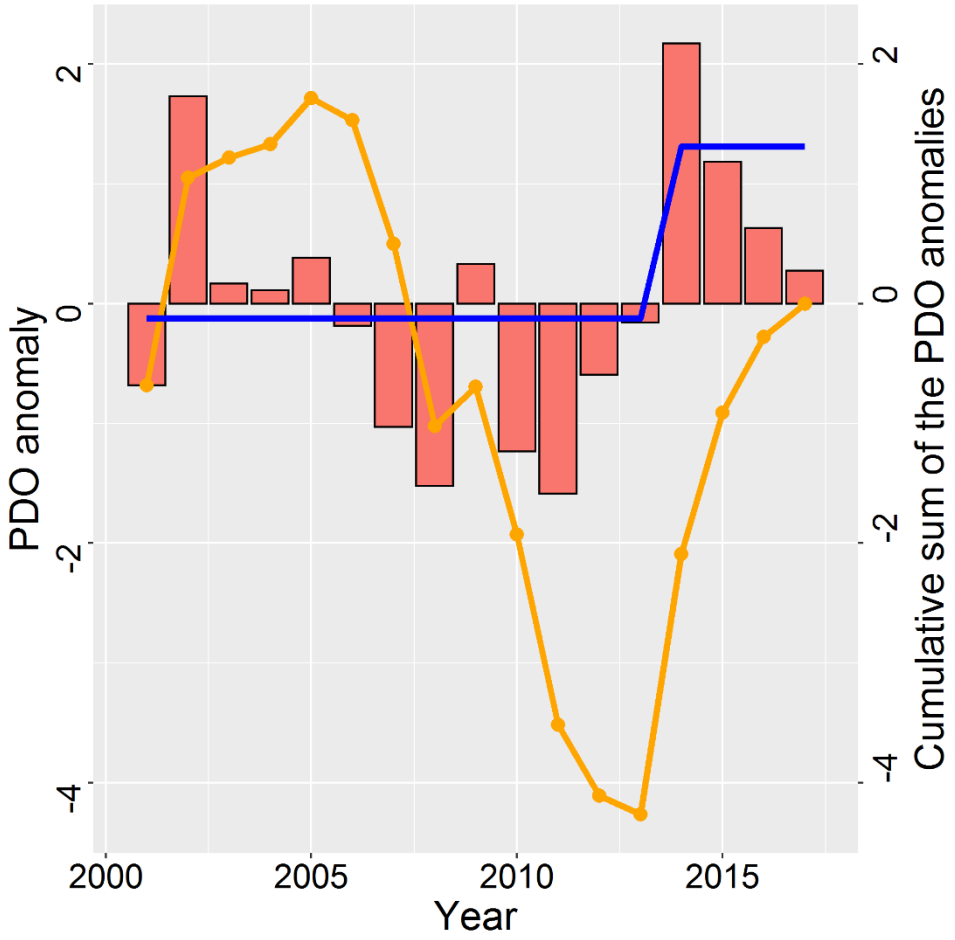
PDO anomaly
2
0
-2
-4
2000
2005
2010
2015
Year
Cumulative sum of the PDO anomalies
2
0
-2
-4